Applied Catalysis B: Environmental 339 (2023) 123100

Contents lists available at ScienceDirect

Applied Catalysis B: Environmental

journal homepage: www.elsevier.com/locate/apcatb

Decipher the key role of ketone toward singlet oxygen evolution in Fenton-like process for water decontamination

Sijin Zuo [a,b,*], Ruixin Guo [a,b], Wendan Xue [c], Jingge Shang [a,b], Jianqiu Chen [a,b,*], Yinqiao Zhang [a,b,*]

[a] State Key Laboratory of Natural Medicines, China Pharmaceutical University, Nanjing 210009, PR China
[b] School of Engineering, China Pharmaceutical University, Nanjing 210009, PR China
[c] Department of Chemistry, Tsinghua University, Beijing 100084, PR China

ARTICLE INFO

Keywords:
Persulfate activation
Metal-free catalyst
Site distance effect
Water remediation
Singlet oxygen

ABSTRACT

Persulfate-based Fenton-like processes are often unsatisfied on the remediation of the complex mediums because the active species of free radicals have usually short lifetime (only 1 μs for hydroxyl radical) or poor selectivity to abatement of the targeted organics. Herein, we report an oxygen-doped carbon catalyst prepared by simple pyrolysis means for persulfate activation to eliminate 2,4-dichlorophenol in the water environment. Experiments and density functional theory calculations uncover reactive sites of the ketonic group displaying the strong site distance effect for the sole active specie of singlet oxygen evolution in the proton-coupled electron transfer regime. Accordingly, the complex water body decontamination has been overwhelmingly realized with the removal efficiency (0.89 (0.007) min^{-1} for 2,4-dichlorophenol), 3.0–9.4 of pH tolerance, the acceptable stability in continuous-flow and cyclic system. Overall, this work provides novel guidance in metal-free persulfate activation systems for real water remediation.

1. Introduction

As one of advanced oxidation processes (AOPs), persulfate (including peroxymonosulfate (PMS) and peroxydisulfate (PDS)) activation-based Fenton-like processes have been always devoted to eliminating the contaminants of environment, and even applying into the tumor therapy in vivo in recent years, by producing the effective active species [1–4]. The active species produced from the process of persulfate activation are usually classified as the free radicals and non-radical species [5]. The common free radicals include hydroxyl radical ($^{\cdot}OH$, 1.8–2.7 V_{NHE}), sulfate radical ($SO_4^{\cdot-}$, 2.5–3.1 V_{NHE}) and superoxide radical ($O_2^{\cdot-}$, −0.28 V_{NHE}) [6–8]. These radicals can directly oxidize and mineralize the organics into harmless intermediates, even water and carbon dioxide [9]. The laboratory-scale treatment of simulated organic wastewater by the free radicals-dominated persulfate activation processes is always high-efficiency. And the dawn for the future application on industrial wastewater remediation seems to be glimpsed. Whereas, due to the active species of free radicals with a short lifetime and blinding attacks, the above technique is difficult to handle the real water bodies which have changeable pH and complex compositions [10,11].

The development or finding of non-radical-dominated Fenton-like reaction broadens the application of persulfate-based Fenton-like technique neared to real water body remediation. These non-radical processes often involve the singlet oxygen ($^1O_2$, 2.2 V_{NHE}), electron transfer process, metastable species, and high-valence metal oxidation [12]. The obvious features of these processes are reaction-mild and high-selective for removal of the targeted organics. Besides, these processes can realize the green and low-cost applications due to the advantages of sufficient utilization of oxidants and the recyclability of reactive sites on the catalysts. Take the reaction process of singlet oxygen as the main active species for example, singlet oxygen with a mild reaction process could avoid the overoxidation of the catalyst. Moreover, it has high selectivity for the electron-rich organics (such as phenolic) by electrophilic addition and electron abstraction, and a long lifetime ranged from 2 to 1000 μs (only 1 μs for $^{\cdot}OH$) [11,13,14]. Accordingly, singlet oxygen-dominated Fenton-like process can well cater to the demand for real water decontamination. Regrettably, the evolution mechanism of singlet oxygen in the persulfate activation process is still controversial [15–17].

An effective method for production of active species of the singlet

* Corresponding authors at: School of Engineering, China Pharmaceutical University, Nanjing 210009, PR China.
E-mail addresses: sjzuo@cpu.edu.cn (S. Zuo), cjqer@163.com (J. Chen), yqzhang@cpu.edu.cn (Y. Zhang).

https://doi.org/10.1016/j.apcatb.2023.123100
Received 23 March 2023; Received in revised form 26 June 2023; Accepted 14 July 2023
Available online 17 July 2023

oxygen on demand in persulfate activation process is the rational design of a catalyst. The widely reported metal-based catalysts for persulfate activation display increasing concerns, for example, difficulty to the cycling of metal valence, easy leaching of metal and high cost in preparation and operation [18,19]. As they are tunable for electron layout, tolerant toward acid and alkaline and easy-accessible in daily life, metal-free carbon catalysts have been expected to overcome the above drawbacks in metal-based catalysts [20]. The heteroatom doping as an effective approach tunes the physicochemical nature of carbon matrix which include physical structure adjusting (such as surface area), defects tailoring and functional group modifying, *etc*. The nitrogen, sulfur and boron are the common heteroatoms for modifying the carbon matrix. However, the oxygen-doped carbon catalysts for high-efficiency Fenton-like process are rarely reported [13], not to mention the deep mechanism excavation for the non-metal-central reactive site with the site distance effect. The adjacent reactive sites display the electronic interaction which is strongly dependent on the site distance [21]. The reactive site with the site distance effect in the metal-based single atom system has been recently evoking an important impact on small molecular activation including persulfate [21], oxygen [22] and hydrogen [23].

Herein we designed and prepared the metal-free oxygen-doped carbon catalyst to active PDS for high-efficiency elimination of the model organic of 2,4-dichlorophenol in water environment. A series of experiments, characterizations, and density functional theory (DFT) calculations were used for thoroughly deciphering the effect of ketonic group for PDS cleavage and sole active species of singlet oxygen evolution. The catalysts with varied site distance of ketone were prepared to investigate the site distance effect on singlet oxygen generation and decontamination performance. The removal of 2,4-dichlorophenol in various actual water bodies and the toxicity assessment of its intermediates were also studied. As far as we know, our work for the first time uncovers the site distance effect in the metal-free catalytic system. This study has a realistic significance for guiding the persulfate-based Fenton-like technique in practical use.

2. Materials and methods

2.1. Chemicals

The chemicals were listed in Text S1 of supplementary material.

2.2. Characterization

The characterizations were recorded in Text S2 of supplementary material.

2.3. Catalyst preparation

First, 30 mg of ketjen black is mixed with 3 mL deionized (DI) water under sonication. After then, 3.5 mmol EDTA, and 65 mmol DCD are added and mixed well with the composites under the sonication and stir. Last, the as-prepared mixture is pyrolyzed for 2 h through 650–900 °C under a nitrogen gas atmosphere with the heating rate of 3 °C/min. The obtained target product is collected for direct use without further treatment. For the descriptor of O/C-T, T is the annealing temperature. For example, the descriptor of O/C-8 denotes the annealing temperature at 800 °C.

To improve the amount of ketonic group of O/C-8, the O/C-8 is modified by the liquid glutaraldehyde [24]. The acquired catalyst is defined as the ketone matched (O/C-8 (M)) for 5 h modified time. Similarly, the ketone overmuch on the O/C-8 (O/C-8 (O)) denotes the modified time of 15 h. For removing ketonic group of catalyst, dansyl hydrazine modification was adopted (see more details in Text S3 and Fig. S1 of supplementary material). The prepared catalyst in this process is called the ketone isolated (O/C-8 (I)).

2.4. Fenton-like experiment

We assessed the catalytic activity of the as-prepared catalysts by the Fenton-like process, in which the catalyst stimulated oxidants (PDS as a model oxidant) to remove the organic contaminants. Fenton-like process was operated in a 50 mL glass beaker's batch apparatus which contained 20 mL, 10 mg/L aqueous solution of organic contaminant (such as, 2,4-dichlorophenol). Sodium hydroxide and sulfuric acid were used to adjust the solution pH if needed. 2 mg catalyst was added into the batch apparatus, then stirred for 30 min to acquire adsorption-desorption equilibrium between the catalyst and organic under magnetic stirring. The Fenton-like reaction was initiated by putting 0.18 mM oxidant into the reactor. 800 μL reaction solution was fetched at designated time and mixed immediately with 200 μL L-histidine (0.2 M) to stop the Fenton-like reaction. The acquired solution was filtered by PTFE filter (0.22 μm) and then sent for HPLC analysis to detect the organic concentration (Text S4). Each experiment of organic degradation was repeatedly conducted at least duplicate to assure the effectiveness of experiment. The removal rate of organics was compared using the pseudo-first-order kinetic model recorded in Text S5.

The H_2O_2 intermediate during Fenton-like process was detected by a modified DPD/POD colorimetric method recorded in Text S6 and Fig. S2 of supplementary material.

3. Results and discussion

3.1. Analysis of morphology and composition of catalyst

Raw materials including ethylene diamine tetraacetic acid (EDTA), dicyandiamide (DCD) and ketjen black (KB) were used to prepare the metal-free oxygen-doped carbon catalyst via a pyrolysis pathway. We have known that ketjen black served as the carbon skeleton due to its natural quality including carbon-only and thermo-stability property, *etc*. [25]. EDTA greatly contributes to the oxygen sources on the carbon skeleton, as its molecular structures shown in Fig. S3. We used the pyrolysis method to modify the carbon motif of ketjen black under the high temperature (800 °C) and inert gas (N_2) protection. It is well known that this method can effectively regulate the electron density of motif by exotic element doping and optimize self-redistribution of structure [11,26].

The morphology of the acquired sample (O/C-8) by SEM characterization is found to be curly, loose and multi-hole (macropores) surface, as displayed in Fig. 1a. This morphology may be attributed to gas (NH_3) volatilization which resulted from the precursor (DCD) pyrolysis [27]. Low-resolution TEM image of O/C-8 catalyst further evidenced the above conclusions (Fig. 1b). Catalyst with this loose and multi-hole construction would provide plenty of sites beneficial to the catalytic oxidizing reaction [28]. High-resolution TEM image (Fig. 1c) shows the multi-layer carbon skeleton and obvious mesopore structures. Notedly, there are unseen lattice fringe on the catalyst in Fig. 1c and halo-like SAED pattern in Fig. 1b inset, both to illustrate the amorphous structure of this O/C-8. Metal-free carbon catalysts with the amorphous features have been reported to benefit charge exchange in catalytic reactions [29]. Elemental analysis including EDS mapping and XPS survey spectrum demonstrates that catalyst O/C-8 contains only three elements of C, N and O, and these elements as well as their functional groups uniformly distribute on the catalyst, as shown in Fig. 1d–g, Fig. S4 and S5a. These results would exclude the possibly metal-involved catalytic process for PDS activation in subsequent reactions.

X-ray diffraction pattern of O/C-8 catalyst displays (002) and (100) plane located respectively at 26.3° and 43.5° (Fig. 1h) demonstrating a carbon construction [30]. The comparably raised peak and smooth peak for respective (002) plane and (001) plane indicate the amorphous and graphitic carbon structure, consistent with the above discussions [31]. In addition, chemical composition of O/C-8 catalyst was analyzed by the XPS technique. As high-resolution XPS spectra of C 1s and O 1s shown

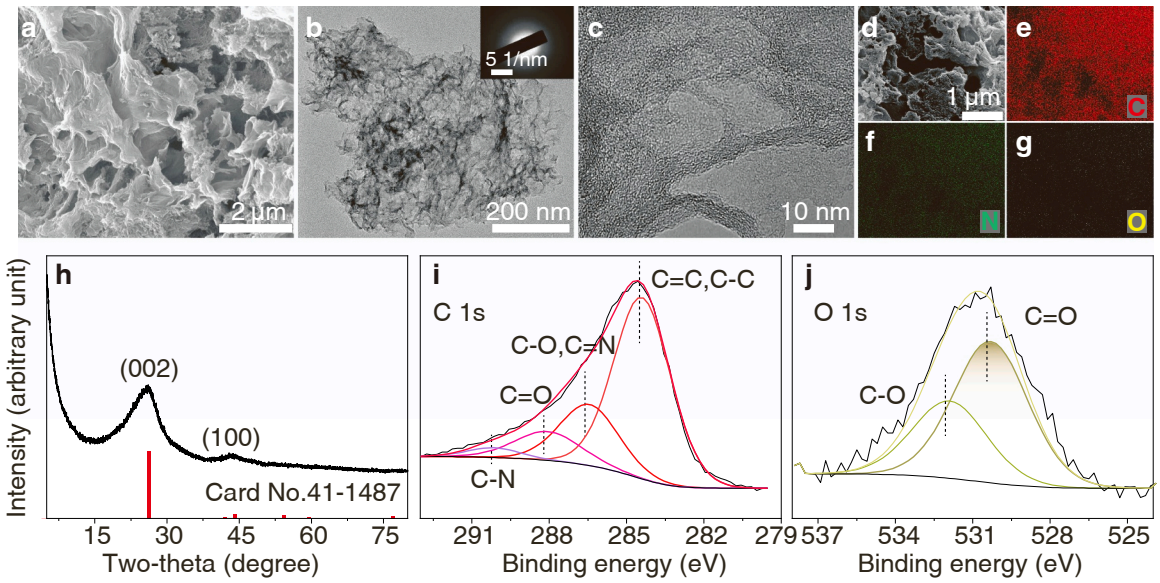

Fig. 1. Characterization of catalyst. a) FE-SEM image of O/C-8 catalyst. b-c) TEM images in b) and selected-area electron diffraction (SAED) pattern in the inset, and high-resolution TEM in c) toward the catalyst of O/C-8. d) SEM image of O/C-8 catalyst. e–g) Elemental mapping image of C, N and O corresponding to the area of Figure d. h) XRD pattern of O/C-8. i and j) High-resolution XPS spectra of C 1s and O 1s toward the catalyst of O/C-8.

respectively in Fig. 1i and j, we can find that carbon is mainly doped by oxygen via bonding with carbon-oxygen covalent bonds and single bonds [32]. Occurrence of carbon-carbon covalent bonds reflected the graphitic degree of carbon-based catalyst to some extent [33]. Accordingly, there are the C═O (530.3 eV) and C—O (531.8 eV) appeared on the catalyst by analyzing the high-resolution O 1s XPS spectra [34].

3.2. Evaluation of Fenton-like performance

We first used O/C-8 activating oxidants to remove the 2,4-dichlorophenol in the water body. 2,4-Dichlorophenol is usually hard-to-remove by AOPs due to the generated chloride ions enabled consuming the active species of free radicals (such as $^{\cdot}OH$) [24,35,36]. To find the optimal oxidant, we tentatively activated common oxidants including peroxide (H_2O_2), PDS and PMS) and periodate via O/C-8 catalyst. The various oxidants activated by O/C-8 catalyst show different performance (Fig. S6a), in which PDS displays the highest reaction rate. This phenomenon is possibly related with the dissociation energy of bond (Fig. S6b) and/or the site distance effect of reactive sites toward oxidants [37–40]. Considering the oxidant's economy and efficacy [41], we chose PDS as an oxidant to explore the reaction process and performance of O/C-8-based system. Key reaction parameters including dosage of

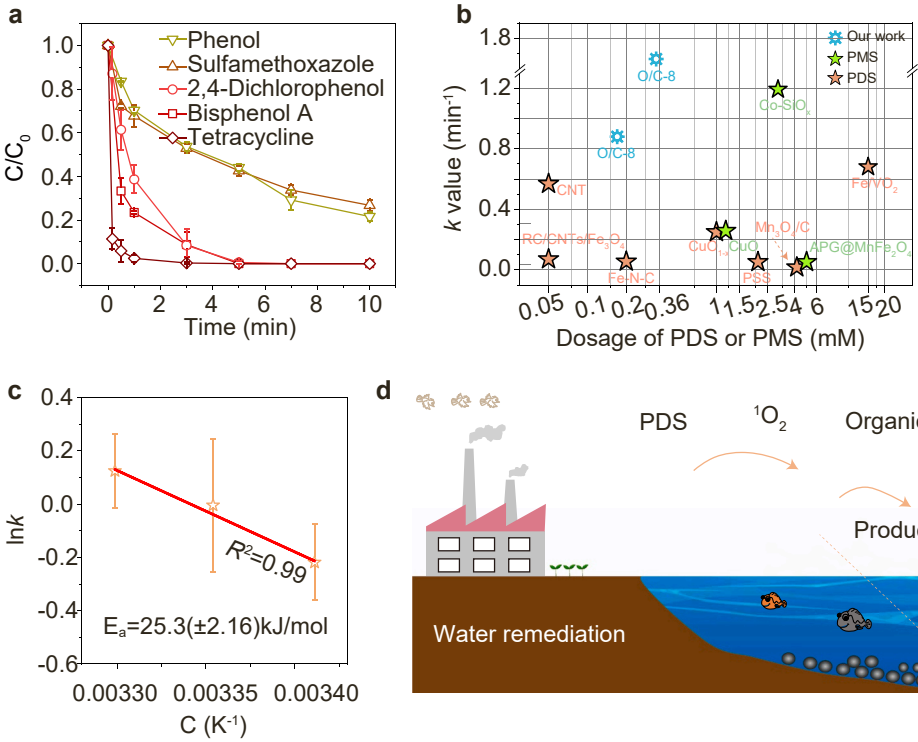

Fig. 2. Catalytic performance of catalyst. a) Performance of various organics removal by O/C-8/PDS system. Reaction conditions: Organics = 10 mg/L, O/C-8 = 0.1 g/L, PDS = 0.18 mM, reaction volume = 20 mL, unadjusted pH, room temperature. b) Comparison of 2,4-dichlorophenol removal with the reported literature. c) Calculation of activation energy (E_a) of O/C-8 catalyst by comparing the relationship between k value and reaction temperature. d) Schematic illustration for the O/C-8/PDS technique in practical application of water remediation.

catalyst and oxidant were respectively optimized (Fig. S7). According to this result, the usage of 0.1 g/L catalyst and 0.18 mM oxidant would be used in subsequent experiments.

A set of organics which have arisen concern toward public health, including phenol compounds (phenol, bisphenol A and 2,4-dichlorophenol) and antibiotic (tetracycline and sulfamethoxazole), were degraded by the designed O/C-8/PDS system. The O/C-8/PDS system has high-efficiency removal for tetracycline (1.29 (+ 0.5) min^{-1}), 2,4-dichlorophenol (0.89 (+ 0.007) min^{-1}) and bisphenol A (0.75 (+ 0.19) min^{-1}) while sluggish removal for phenol and sulfamethoxazole (Fig. 2a and Fig. S8). These results interpreted that active species produced only by O/C-8/PDS pairs is selective to organic degradation. Besides, we compared these *k* values with the reported works under similar reaction conditions and displayed in Fig. 2b and Table S1. Our work for removal of 2,4-dichlorophenol shows a record-breaking performance. We calculated the activation energy (E_a) of O/C-8/PDS system under different reaction temperatures (Text S7, Fig. S9 and Fig. 2c). The calculated E_a is 25.3(+ 2.16) kJ/mol, demonstrating a quite low reaction barrier compared with the reported works (Fig. S10). Thereof, our O/C-8/PDS based Fenton-like system is hopeful to further use in practical site remediation (Fig. 2d).

3.3. *Identifying the site distance effect of reactive site*

To deep decipher the reaction process, a set of catalysts (O/C-T, T denotes the pyrolysis temperature) were first prepared, used for organic

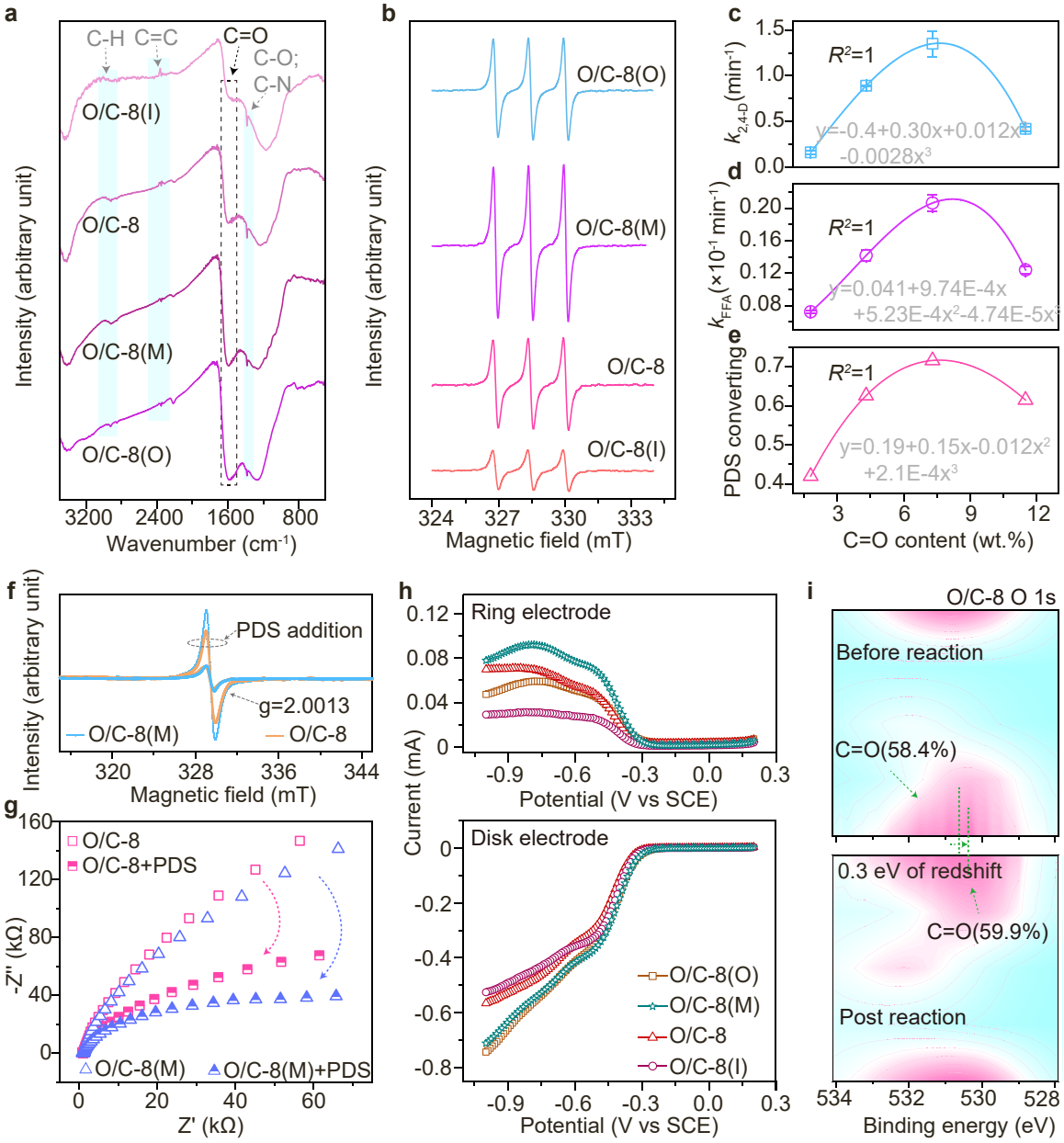

Fig. 3. Exploration of catalytic sites and its site distance effect. a) FTIR spectra of O/C-8 (I), O/C-8, O/C-8 (M) and O/C-8 (O). b) EPR spectra for comparison of active species concentration in O/C-8 series with various ketonic group content activating PDS system. Comparison and fitting among the amount of ketonic group on the O/C-8 series detected by XPS technique and these catalysts activated PDS for c) 2,4-dichlorophenol removal rate ($k_{2,4-D}$), d) furfuryl alcohol removal rate (k_{FFA}) and e) for PDS converting. f) EPR spectra of catalysts with or without mixing of PDS to detect the electronic interaction between catalysts and oxidant. g) Electrochemical impedance spectroscopy of catalysts with the present or absent PDS. h) A rotating ring-disk electrode combined with the electrochemical workstation to detect the oxidant (PDS) reduction on the disk electrode and its products oxidation on the ring electrode under the inert atmosphere. i) O 1s high-resolution XPS spectra of pristine O/C-8 and used O/C-8.

degradation by PDS activation. The furfuryl alcohol (FFA) was selected as a probe organic due to its high reaction rate constants with the common active species in activation of persulfate-based system, such as $>10^8$ $M^{-1}s^{-1}$ with $^{\cdot}OH$, $SO_4^{\cdot-}$ or $^1O_2$ [42]. The experimental results show that furfuryl alcohol can be effectively degraded (Fig. S11a), as well as the improved removal rate with the increasing annealing temperature for O/C-T catalyst (Fig. S11b). The negligible adsorption of furfuryl alcohol by O/C-T series (Fig. S12) indicates furfuryl alcohol removal was contributed to catalytic oxidizing without any adsorption contribution. This finding would eliminate the possible distractors from the else factors of non-reactive sites, such as physical construction of catalysts. We had screened the chemical composition of catalysts, and found that the ketonic group of catalyst has played a vital role for PDS activation. In order to acquire an effective conclusion, we measured the ketonic group content using the XPS technique and the fluorescence labelling of dansyl hydrazine. The ketone content ranged from 1.00 wt% to 4.34 wt% measured by XPS technique or increased from 3.55 μg/g to 4.51 μg/g measured by fluorescence labelling, with the increasing annealing temperature (Fig. S13, Table S2 and Fig. S14). It should be noted that the ketone content measured by the two methods both matches well with furfuryl alcohol removal (*k* value) (Fig. S15). This finding confirms the ketonic group as the reactive sites for PDS activation.

According to this clue, we subsequently added or eliminated the amount of ketonic group of O/C-8 by the glutaraldehyde or dansyl hydrazine modifying, respectively (see the text of Catalyst preparation). As expected, the acquired results (Fig. S16-S18) demonstrate the ketone content for the catalysts increased from O/C-8 (I), O/C-8, O/C-8 (M) to O/C-8 (O). For example, the ketone content increased from 1.83 wt% to 11.54 wt% for the catalysts of ketone isolated (O/C-8 (I)) and ketone overmuch (O/C-8 (O)) respectively, quantified by the XPS technique. Besides, the characterization of FITR for these catalysts in Fig. 3a also proves this. The ketone stretching located at wavenumber of 1562–1620 cm^{-1} is obviously enhanced for the catalysts from O/C-8 (I) to O/C-8 (O). However, else stretching such as carbon-carbon/oxygen bonds, representing the graphitization or defects of catalysts, *etc*. [43], displays a negligible change possibly due to the mild surface-modification means of these catalysts. This result indicates that the defects or graphitization degree would not be a possible reactive site. These characterizations all prove the tunable ketone content on the catalyst. The ketone content of O/C-8 can be described by the site distance of ketonic group because of the even distribution of functional group. The increased content hints the decreased site distance of ketonic group. The site distance of ketonic group has a vital effect on generating active species by PDS activation. This view is first confirmed by electron paramagnetic resonance (EPR) technique using 2,2,6,6-tetramethyl-4--piperidinol (TEMP) as a spin-trapping agent for possible active species adducts. As demonstrated in Fig. 3b, we found the increased signal intensity of EPR with the decreased site distance of ketone from O/C-8(I) to O/C-8(M), and the decreased signal intensity from O/C-8(M) to O/C-8 (O). This result indicates the ketonic group matched for PDS activation can produce more active species. Nevertheless, the overmuch ketonic group would weaken the production of active species. The varied site distance of ketonic group activating PDS systems were used to degrade 2,4-dichlorophenol (Fig. S19) and furfuryl alcohol (Fig. S20). Both can be effectively degraded, and the removal rate is dependent on the site distance of ketonic group. When the site distance of ketonic group decreased to gradually match the symmetric PDS molecular, the more effective PDS activation processes would occur [21]. However, the overmuch ketonic group on the catalyst would possibly distract for PDS adsorption and activation process. The result of PDS converting by the varied site distance of ketonic group could evidence the above view (Fig. S21 and Text S8). Moreover, we found the perfectly fitting ($R^2 = 1$) among removal rate ($k_{2,4-D}$ and k_{FFA}), PDS converting and the site distance effect of ketonic group using a polynomial equation as demonstrated in Fig. 3c, d, e and Fig. S22. This phenomenon further demonstrates the site distance effect of ketonic group affecting PDS activation. A similar phenomenon to the site distance of reactive site was reported in the metal-based single atom system [21,22]. It is worth to declare that this work for the first time found the site distance effect in the metal-free system.

Subsequently, we explored the electronic interaction between the site distance effect of ketonic group and PDS activation by experiments and DFT calculations. EPR spectra of Fig. 3f display an obvious signal and similar intensity at $g = 2.0013$ for the two samples of O/C-8 and O/C-8 (M), which was attributed to the unpair electron in the carbon substrate [44]. After mixing with PDS, the increased intensity of EPR signal is observed. And the signal intensity of O/C-8 (M)/PDS is higher than the O/C-8/PDS. This finding affirms the electronic interaction between the catalyst and PDS, as well as the site distance of ketonic group affecting the electronic interaction. This process was also explored by a set of electrochemical experiments (see more experimental details in Text S9 of supplementary material). Electrochemical impedance spectroscopy of O/C-8 series in Fig. 3g and Fig. S23 implies the increased electron transfer rate on the interface resistance after adding PDS, particularly when PDS encounters the proper site distance of ketonic group [45]. A rotating ring-disk electrode (RRDE) test was used to explore the PDS decomposition by the varied ketonic group of O/C-8 series (Fig. S24). The electrolyte contained the saturated inert gas and a certain amount of PDS. As can be seen in Fig. 3h, the increased reduction current on the disk electrode along with the decreased site distance of ketone. It indicates the more beneficial electron transfer caused by the increased ketone content. However, the oxidation currents of reduction products are different on the ring electrode, on which the current from O/C-8 (I) to O/C-8 (M) increased in turn while O/C-8 (O) dropped. This result elaborates mightily that the site distance of ketonic group has an important effect for PDS activation. Furthermore, we compared the high-resolution O 1s XPS spectra of O/C-8 pristine and used in the long operation by a continuous apparatus (Fig. 6e vide infra), as shown in Fig. 3i and Fig. S25. The stable amount of ketonic group (58.4 %→59.9 %) occurred the slight 0.3 eV redshift of binding energy. These experiment results collectively point out that the ketonic group of catalyst would show the closely electronic interaction with PDS, especially when PDS encountered the proper site distance of ketonic group.

O/C-8 serials with the varied site distance of ketone were named as ketone isolated, ketone matched and ketone overmuch. And they were modeled by the amount of ketonic group in DFT calculation, as demonstrated in Fig. 4a. The result shows that the S-O_β bond of PDS is easily stretched when PDS encountered the ketone with the decreased site distance. For instance, S-O_β bonds of PDS after encountering the ketone isolated and ketone matched are 1.995 Å and 2.030 Å, respectively, while O_β-O_β bond lengths are respectively 1.323 Å and 1.317 Å (Fig. 4a and Fig. S26). This phenomenon in our research is different from the widely reported similar works, in which the preferential break is O_β-O_β in PS (Table S3). It could be explained by the adsorption energy between the reactive sites of ketonic group with the varied site distance effect and PDS molecular. As demonstrated in Fig. 4b and Table S4, we found that the adsorption energy between ketone matched and PDS is the highest (−0.95 eV), and ketone overmuch and isolated are decreased in sequence. Additionally, projected crystal orbital Hamilton populations (pCOHP) as a potent instrument to explore the bonding interaction between PDS and reactive sites of ketonic group, were used as demonstrated in Fig. 4c. The bonding orbital all nearly locates below the Fermi level for the catalyst of ketone matched than that of ketone isolated and ketone overmuch, to indicate the more bonding interaction for PDS molecular by the former. Taking antibonding orbital into consideration, the integrated COHP (ICOHP) was introduced to quantitatively illustrate the strength of bonding interaction between PDS and catalyst. The calculated ICOHP values for the ketone isolated, ketone matched and ketone overmuch are respectively − 2.90, − 2.93 and − 2.94 to suggest that the decreased site distance of ketonic group intensively interacted with the PDS molecular. This result is in accordance with the disk electrode test of the varied ketone content of catalysts by RRDE

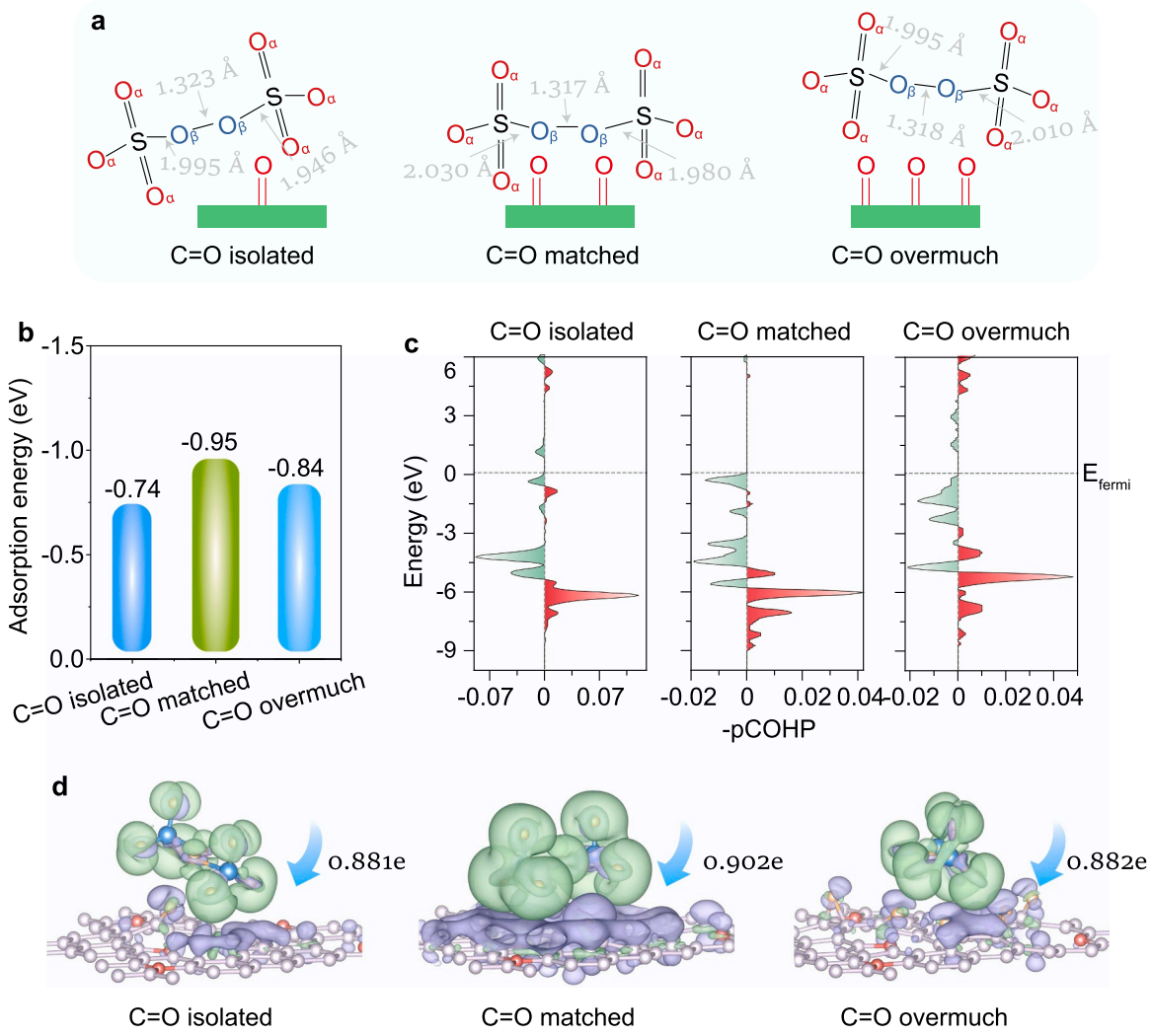

Fig. 4. DFT calculation for uncovering the site distance effect of ketonic group. a) Bond length of PDS after contacting the reactive sites of ketonic group with isolated, matched and overmuch, respectively. b) Adsorption energy between PDS and the corresponding catalytic sites in a). c) Projected crystal orbital Hamilton populations between catalysts and PDS molecular. d) Charge density difference and Bader charge toward the electron transfer analysis between catalysts and PDS. The indigo blue and the green represent respectively the electron accumulation and depletion.

shown in Fig. 3 h. ICOHP value of the ketone matched is not the most negative among the three models, possibly indicating that the charge exchange is also important except for the bonding interaction. We used the charge density difference and the Bader charge analysis to simulate the charge exchange in the above three models, as demonstrated in Fig. 4d. The results show that the electron transfer from PDS to the ketonic group is apt to occur and the highest value of 0.902e for the ketone matched is observed. This observation is respectively in line with the EPR analysis in Fig. 3f, the ring electrode test in Fig. 3h and O 1s high-resolution XPS spectra in Fig. 3i. DFT calculation further verified the site distance effect of ketonic group during PDS activation process.

3.4. Identifying the active species and its evolution pathway

Methanol is an effective trapping agent for free radicals ($^{\cdot}OH$ and $SO_4^{\cdot-}$) due to the quick reaction rate with $^{\cdot}OH$ ($9.7 \times 10^8\ M^{-1}s^{-1}$) and $SO_4^{\cdot-}$ ($1.1 \times 10^7\ M^{-1}s^{-1}$) [46]. 100 mM methanol was put into the present system yet displayed insignificant disturbance toward organic abatement (Fig. S27a and Fig. 5a). This result confirmed the free radicals did not participate in organic removal in our system. Molecular probe experiments (Fig. S28) and EPR analysis (Fig. S29 and S30) support this view. We hence turned more think on the possible non-radicals-based reaction pathway. L-histidine is a classic singlet oxygen quencher because of high reaction rate with singlet oxygen ($1.5 \times 10^8\ M^{-1}s^{-1}$) [47]. When L-Histidine was added into the reaction system, 2,4-dichlorophenol removal was almost stagnant (Fig. S27a and Fig. 5a). Besides, β-carotene, as another famous trapping agent for singlet oxygen ($2–3.0 \times 10^{10}\ M^{-1}s^{-1}$) [48], was used to observe the similar quenching effect (Fig. S27b). Considering its insolubility in water (0.6 mg per liter water at 298.15 K) and easy solubility in acetone, we replaced the reaction solution of water with 50 % acetone aqueous [49]. These phenomena all evidenced the effectiveness of quenching experiment and collectively pointed out the singlet oxygen as active species in our system. EPR technique was further used to tamp this conclusion. An obvious triplet peak with the intensity ratio of 1:1:1 which indicated the presence of TEMPO from TEMP-singlet oxygen adducts was observed in O/C-8 and PDS coexisting EPR spectrum (Fig. S29a and Fig. 5b). These EPR results supported the discussion of Fig. 2a and Fig. S8. Our experiments and discussions denied another possible active species in this system. The reported high valent active species were also excluded by the PMSO oxygen transferred experiment (Fig. S31). There lack the metastable complexes and electron transfer process which occurs between organic and oxidant assisted by the bridge of catalyst, due to PDS effectively converting under the absent organics (vide discussion of PDS

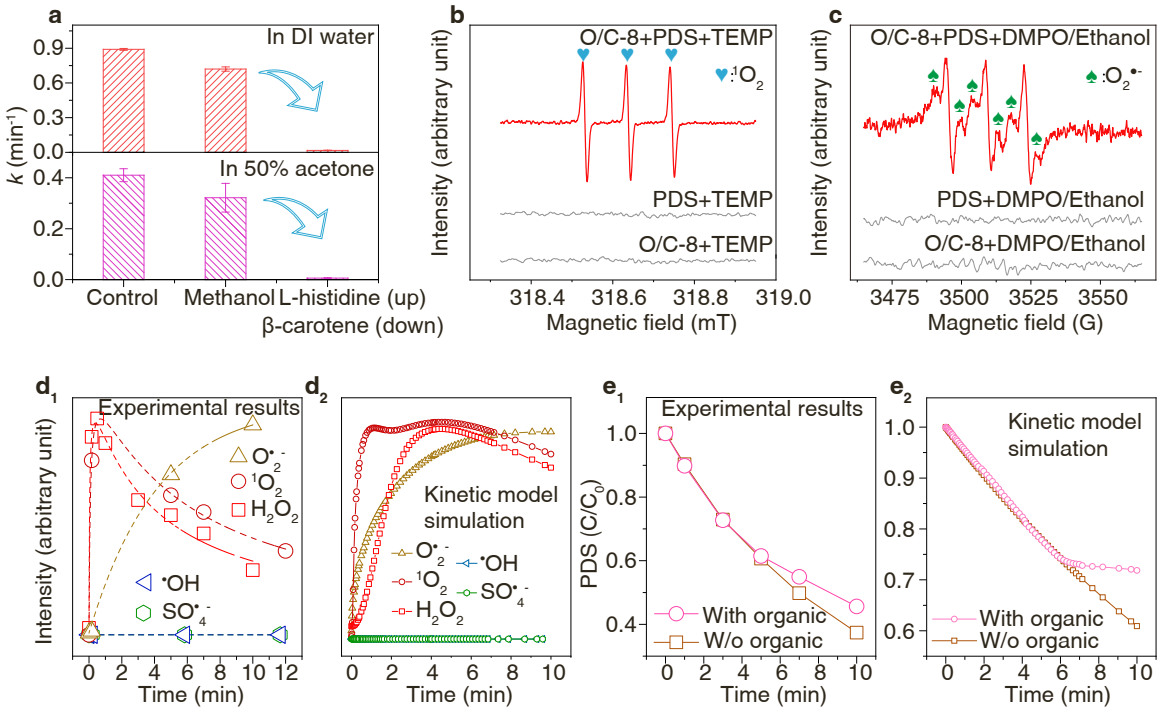

Fig. 5. Exploration of active species. a) Comparison of *k* value of 2,4-dichlorophenol removal in control group and adding scavenger group, including free radicals trapping agent (methanol) and singlet oxygen quencher (L-histidine and β-carotene). b) EPR spectra for detection of singlet oxygen by adding TEMP as spin-trapping agent under different reaction conditions. c) EPR spectra for detection of superoxide radical by adding DMPO as spin-trapping agent in containing ethanol solution. d_1) The experimental results recorded the intensity of active species including $^{\cdot}OH$, $SO_4^{\cdot-}$, $O_2^{\cdot-}$, H_2O_2 and $^1O_2$. d_2) The kinetic model predicted the intensity of active species including $^{\cdot}OH$, $SO_4^{\cdot-}$, $O_2^{\cdot-}$, H_2O_2 and $^1O_2$. e_1) The experimental results recorded the concentration change of PDS oxidant in the present and absent of organic by using the potassium iodide colorimetry. e_2) The kinetic model predicted the concentration change of PDS oxidant in the present and absent of organic.

decomposition infra). Overall, all experiments demonstrated singlet oxygen as the sole active species worked for organic abatement.

Many endeavors have been made to explore the evolution pathway of singlet oxygen in our system. Superoxide radical could serve as the precursor of singlet oxygen generation considering the viable thermodynamic process ($E(O_2^{\cdot-}/^1O_2) = -0.34\ V_{NHE}$) [50]. We used 5, 5-dimethyl-1-pyrroline *N*-oxide (DMPO) as a spin-trapping agent for detection of the superoxide radical ($O_2^{\cdot-}$) in EPR technique (Fig. S29b) [51]. The obvious signal of sextet peak identified as the adduct of DMPO-$O_2^{\cdot-}$ was found to hint the existence of superoxide radical (Fig. 5c). In addition, the trapping of superoxide radical by adding $CHCl_3$ scavenger ($k_{O_2^{\cdot-}+CHCl_3} = 3 \times 10^{10}\ M^{-1}s^{-1}$) manifests that the superoxide radical has a vital role in the evolution of singlet oxygen (Fig. S32) [52]. We found accidentally a slight generation of hydrogen peroxide in O/C-8/PDS system (Fig. 5d_1, d_2 and Table S7). However, after trapping the superoxide radical, hydrogen peroxide and singlet oxygen both were disappeared (Fig. S33). These findings enlightened that hydrogen peroxide was produced as the concomitant product of singlet oxygen. The experimental result in Fig. S6a and hydrogen peroxide trapping by adding catalase (Fig. S34) both excluded the possibility of hydrogen peroxide activated by O/C-8 catalyst. The dissolved oxygen was proved not to participate in the generation of singlet oxygen through the experiment of 2,4-dichlorophenol degradation under the absent oxygen atmosphere (Fig. S35). Based on the above analysis, there are enough reasons to approve the view that the superoxide radical as intermediates was transformed into singlet oxygen.

The reaction solution of absolute water was replaced by a half-volume water solution resulting in a significant decrease of 2,4-dichlorophenol removal (Fig. S27b). And pH value was enhanced during the Fenton-like reaction process (Fig. S36). Both indicate the vital role of water as a possible proton donor for singlet oxygen generation. Moreover, we explored the role of electrons by the experiment of adding the trapping agent of $AgNO_3$ shown in Fig. S37. This result again highlights the intrinsic electron transfer mechanism between the PDS molecular and reactive site of the ketonic group.

Last, PDS converting during the reaction process was detected and simulated (Fig. 5e_1 and Fig. 5e_2). More than 60 % PDS converting by low-dosage O/C-8 catalyst (0.1 g/L) not only indicates the high-efficiency utilization of oxidant to save cost, but also could avoid the excessive oxidation of catalyst to promote stability. When 2,4-dichlorophenol presented in the process, PDS converting seemed to turn slow. This phenomenon demonstrated the steric hindrance between organic and oxidant and hinted that the reactive sites of ketone activating oxidant to remove organic occur on the surface of O/C-8 instead of the bulk solution. This explanation can be supported by the above DFT calculation. Overall, the proton-coupled electron transfer process was comprehensively presented in this system.

3.5. *Practical application of technique and toxicity assessment of intermediates*

Possible practical application of this technique was tested under different scenes. Fig. 6a shows the pH tolerance of O/C-8/PDS system ranging from 3.0 to 9.4. It is capable to adapt most of wastewater pH. The slightly enhanced treatment performance with the increased pH value is attributed to that singlet oxygen has a higher oxidation potential under a higher pH [53]. Disturbance of inorganic ions and humic acid for this system was tested and shown in Fig. 6b. Cl^- did not affect 2, 4-dichlorophenol removal in our singlet oxygen-dominated reaction process. Cl^- has more disturbance for $^{\cdot}OH$ and $SO_4^{\cdot-}$ based Fenton-like system due to the quick reaction between Cl^- and $^{\cdot}OH$ ($4.3 \times 10^9\ M^{-1}\ s^{-1}$), Cl^- and $SO_4^{\cdot-}$ ($3.0 \times 10^8\ M^{-1}\ s^{-1}$) [54]. Humic acid, CO_3^{2-} and HCO_3^- displayed much slight effect for 2,4-dichlorophenol removal due to the possible steric hindrance of those matters, indicating the above-mentioned surface-occurred redox reaction. Furthermore, our system for

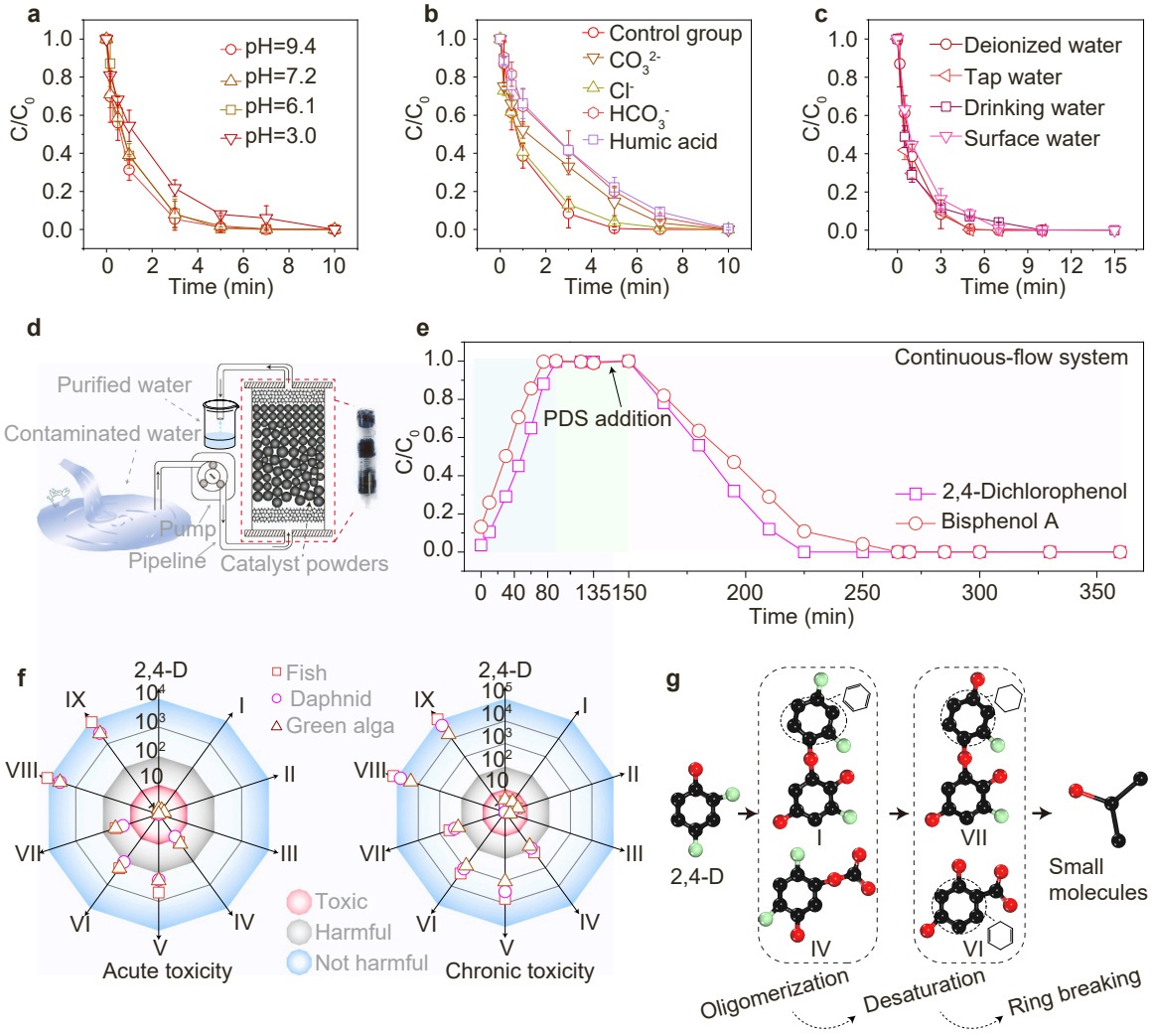

Fig. 6. Practical application of O/C-8/PDS technique and toxicity evaluation of intermediates during the process of organic degradation. a) 2,4-Dichlorophenol degradation by O/C-8/PDS system under different pH values. b) 2,4-Dichlorophenol degradation by O/C-8/PDS system affected by inorganic ions (CO_3^{2-}, HCO_3^- and Cl^-), and humic acid. Reaction conditions: 2,4-dichlorophenol= 10 mg/L, O/C-8 = 0.1 g/L, PDS= 0.18 mM, reaction volume= 20 mL, unadjusted pH, room temperature, Na_2CO_3 = $NaHCO_3$ = NaCl = humic acid = 5 mM (if needed). c) Removal of 2,4-dichlorophenol in various real water bodies including tap water, drinking water and surface water. d) Schematic illustration of continuous flow apparatus. e) Removal of 2,4-dichlorophenol and bisphenol A by O/C-8 constructed continuous flow system. Reaction conditions: O/C-8 = 40 mg, 2,4-dichlorophenol=bisphenol A= 5 mg/L, flow rate= 4 mL/min, PDS= 1 mM. f) Toxicity analysis of intermediates from 2,4-dichlorophenol degradation, including acute toxicity and chronic toxicity. Red, gray and green background respectively denotes the toxic, the harmful and the not harmful. Rectangle, circle and triangle represents respectively the toxicity to fish, daphnid and green alga. g) Analysis of degradation process of 2,4-dichlorophenol.

2,4-dichlorophenol remove in different real water bodies, including drinking water, tap water and lake water, all showed an excellent purification performance (Fig. 6c). These water quality parameters were listed in Table S5 of supplementary material. We constructed a continuous-flow system using a syringe in which the O/C-8 catalyst was stabilized at the middle of syringe, while both ends of the syringe were plugged by the polyurethane foam to prevent the leaching of catalyst along with the water flow (Fig. 6d). The contaminated water mixed with PDS oxidant was pumped by a peristaltic pump to be degraded after contacting the catalyst. The experimental results show that the effluent concentration of 2,4-dichlorophenol and bisphenol A both obviously dropped until to near zero and kept continuously this state around 210 min. The cyclic stability experiment of O/C-8/PDS system (Fig. S38) and characterizations (Fig.S39) of the microstructure and chemical composition for O/C-8 post reaction all corroborate the acceptable stability of this system. Thus, these results demonstrate the hopeful practical use of this system.

Considering mineralization (Fig. S40) and dechlorination (Fig. S41) of 2,4-dichlorophenol both slower than itself degradation, we further explored the possible products of 2,4-dichlorophenol degradation using the LC/MS technique. The result in Fig. S42 displays that there are possible ten intermediates in degradation process. The acute and chronic toxicity of these intermediates were evaluated by the predictive model of Ecological Structure Activity Relationships (ECOSAR) [55]. The results of the predictive model indicated that the acute and chronic toxicity of intermediates both gradually decreased as displayed in Fig. 6f and Table S6. We put a possible pathway of 2,4-dichlorophenol degradation in Fig. 6g and Fig. S43 according to the acquired evidence and reported works [56]. 2,4-Dichlorophenol first undergone a self-coupling reaction to transform the dimer under the mild oxidizing system. Next, the dimer and/or 2,4-dichlorophenol matrix were further oxygenated for desaturation. Subsequently, they proceeded to the ring opening to generate the small molecules, such as oxalic acid, formic acid, and so on, eventually mineralized into water and carbon dioxide.

4. Conclusions

This work reported a metal-free oxygen-doped carbon catalyst for PDS activation to remove organics in water. A simple pyrolysis process was used for preparing the targeted catalyst. The important role of ketone on the catalyst to display the site distance effect for generating the active species of singlet oxygen in PDS activation was identified. The record-breaking catalytic performance for organic removal by our system is attributed to the low activation energy of the catalyst (25.3 (+ 2.16) kJ/mol) and high-efficiency utilization of oxidant, *etc*. This metal-free technique is effective for real water remediation to avoid the re-contamination caused by the metal-based system. This work provides a novelty insight on the technique of persulfate activation for real water remediation.

CRediT authorship contribution statement

Sijin Zuo: Investigation, Methodology, Writing – original draft, Funding acquisition, Writing – review & editing. **Ruixin Guo:** Resources, Data curation. **Wendan Xue:** Resources. **Jingge Shang**: Investigation. **Jianqiu Chen:** Funding acquisition, Supervision. **Yinqiao Zhang:** Conceptualization, Supervision, Funding acquisition, Writing – review & editing.

Declaration of Competing Interest

The authors state no competing interests.

Data Availability

Data will be made available on request.

Acknowledgements

The authors thank the funding supported by the High-Level Talent Introduction Project of China Pharmaceutical University (No. 3150110052 and No. 3150110051).

Appendix A. Supporting information

Supplementary data associated with this article can be found in the online version at doi:10.1016/j.apcatb.2023.123100.

References

[1] B.C. Hodges, E.L. Cates, J.H. Kim, Challenges and prospects of advanced oxidation water treatment processes using catalytic nanomaterials, Nat. Nanotechnol. 13 (2018) 642–650, https://doi.org/10.1038/s41565-018-0216-x.

[2] X.D. Zhang, J. Wang, B.B. Xiao, Y.J. Pu, Y.C. Yang, J.S. Geng, D.Y. Wang, X.J. Chen, Y.X. Wei, K. Xiong, Y.F. Zhu, Resin-based photo-self-Fenton system with intensive mineralization by the synergistic effect of holes and hydroxyl radicals, Appl. Catal. B: Environ. 315 (2022), 121525, https://doi.org/10.1016/j.apcatb.2022.121525.

[3] Y. Liu, W.Y. Zhen, Y.H. Wang, S.Y. Song, H.J. Zhang, $Na_2S_2O_8$ Nanoparticles trigger antitumor immunotherapy through reactive oxygen species storm and surge of tumor osmolarity, J. Am. Chem. Soc. 142 (2020) 21751–21757, https://doi.org/10.1021/jacs.0c09482.

[4] W. Liu, P. Fu, Y. Zhang, H. Xu, H. Wang, M. Xing, Efficient hydrogen production from wastewater remediation by piezoelectricity coupling advanced oxidation processes, Proc. Natl. Acad. Sci. USA 120 (2023), e2218813120, https://doi.org/10.1073/pnas.2218813120.

[5] Z.Y. Guo, Y. Si, W.Q. Xia, F. Wang, H.Q. Liu, C. Yang, W.J. Zhang, W.W. Li, Electron delocalization triggers nonradical Fenton-like catalysis over spinel oxides, Proc. Natl. Acad. Sci. USA 119 (2022), e2201607119, https://doi.org/10.1073/pnas.2201607119.

[6] Y. Nosaka, A.Y. Nosaka, Generation and detection of reactive oxygen species in photocatalysis, Chem. Rev. 117 (2017) 11302–11336, https://doi.org/10.1021/acs.chemrev.7b00161.

[7] J. Cao, W.S. Nie, L. Huang, Y.B. Ding, K.L. Lv, H.Q. Tang, Photocatalytic activation of sulfite by nitrogen vacancy modified graphitic carbon nitride for efficient degradation of carbamazepine, Appl. Catal. B: Environ. 241 (2019) 18–27, https://doi.org/10.1016/j.apcatb.2018.09.007.

[8] X.Y. Liu, X.Y. Yan, W.Y. Liu, Q.Y. Yan, M.Y. Xing, Switching of radical and nonradical pathways through the surface defects of Fe_3O_4/MoO_xS_y in a Fenton-like reaction, Sci. Bull. 68 (2023) 603–612, https://doi.org/10.1016/j.scib.2023.02.031.

[9] X.F. Xiang, L.Y. Wu, J.J. Zhu, J.Z. Li, X. Liao, H.C. Huang, J.J. Fan, K.L. Lv, Photocatalytic degradation of sulfadiazine in suspensions of TiO_2 nanosheets with exposed (001) facets, Chin. Chem. Lett. 32 (2021) 3215–3220, https://doi.org/10.1016/j.cclet.2021.03.064.

[10] L.S. Zhang, X.H. Jiang, Z.A. Zhong, L. Tian, Q. Sun, Y.T. Cui, X. Lu, J.P. Zou, S. L. Luo, Carbon nitride supported high-loading Fe single-atom catalyst for activating of peroxymonosulfate to generate $^1O_2$ with 100 % selectivity, Angew. Chem. Int. Ed. 60 (2021) 21751–21755, https://doi.org/10.1002/anie.202109488.

[11] X.N. Li, X. Huang, S.B. Xi, S. Miao, J. Ding, W.Z. Cai, S. Liu, X.L. Yang, H.B. Yang, J. J. Gao, J.H. Wang, Y.Q. Huang, T. Zhang, B. Liu, Single cobalt atoms anchored on porous N-doped graphene with dual reaction sites for efficient Fenton-like catalysis, J. Am. Chem. Soc. 140 (2018) 12469–12475, https://doi.org/10.1021/jacs.8b05992.

[12] J.Q. Ji, X.Z. Yuan, Y.L. Zhao, L.B. Jiang, H. Wang, Mechanistic insights of removing pollutant in adsorption and advanced oxidation processes by sludge biochar, J. Hazard. Mater. 430 (2022), 128375, https://doi.org/10.1016/j.jhazmat.2022.128375.

[13] J.F. Yu, H.P. Feng, L. Tang, Y. Pang, G.M. Zeng, Y. Lu, H.R. Dong, J.J. Wang, Y. N. Liu, C.Y. Feng, J.J. Wang, B. Peng, S.J. Ye, Metal-free carbon materials for persulfate-based advanced oxidation process: microstructure, property and tailoring, Prog. Mater. Sci. 111 (2020), 100654, https://doi.org/10.1016/j.pmatsci.2020.100654.

[14] X.Y. Mi, P.F. Wang, S.Z. Xu, L.N. Su, H. Zhong, H.T. Wang, Y. Li, S.H. Zhan, Almost 100 % Peroxymonosulfate conversion to singlet oxygen on single-atom CoN_{2+2} Sites, Angew. Chem. Int. Ed. 60 (2021) 4588–4593, https://doi.org/10.1002/anie.202014472.

[15] Y.C. Deng, Z.P. Zhou, H. Zeng, R.D. Tang, L. Li, J.J. Wang, C.Y. Feng, D.X. Gong, L. Tang, Y. Huang, Phosphorus and kalium co-doped g-C_3N_4 with multiple-locus synergies to degrade atrazine: insights into the depth analysis of the generation and role of singlet oxygen, Appl. Catal. B: Environ. 320 (2023), 121942, https://doi.org/10.1016/j.apcatb.2022.121942.

[16] N.C. Zheng, X. He, R.T. Hu, R.L. Wang, Q. Zhou, Y.K. Lian, Z.F. Hu, In-situ production of singlet oxygen by dioxygen activation on iron phosphide for advanced oxidation processes, Appl. Catal. B: Environ. 307 (2022), 121157, https://doi.org/10.1016/j.apcatb.2022.121157.

[17] J.L. Zheng, Q.T. Lin, Y.X. Liu, X.D. Fan, K.H. Xu, Y.J. Ma, J. He, H.Y. Fu, Peroxymonosulfate activation by Mg-introduced Fe-N carbon nanotubes to accelerate sulfamethoxazole degradation: Singlet oxygen-dominated nonradical pathway, Chem. Eng. J. 452 (2023), 139233, https://doi.org/10.1016/j.cej.2022.139233.

[18] Y.H. Li, D.Y. Lin, Y.F. Li, P.K. Jiang, X.B. Fang, B. Yu, Nonradical-dominated peroxymonosulfate activation through bimetallic Fe/Mn-loaded hydroxyl-rich biochar for efficient degradation of tetracycline, Nano Res. 16 (2022) 155–165, https://doi.org/10.1007/s12274-022-4640-8.

[19] S.J. Zuo, X.M. Jin, X.W. Wang, Y.H. Lu, Q. Zhu, J.W. Wang, W.P. Liu, Y.H. Du, J. Wang, Sandwich structure stabilized atomic Fe catalyst for highly efficient Fenton-like reaction at all pH values, Appl. Catal. B: Environ. 282 (2021), 119551, https://doi.org/10.1016/j.apcatb.2020.119551.

[20] X.G. Duan, H.Q. Sun, S.B. Wang, Metal-free carbocatalysis in advanced oxidation reactions, Acc. Chem. Res. 51 (2018) 678–687, https://doi.org/10.1021/acs.accounts.7b00535.

[21] B. Wang, C. Cheng, M. Jin, J. He, H. Zhang, W. Ren, J. Li, D. Wang, Y. Li, A site distance effect induced by reactant molecule matchup in single-atom catalysts for Fenton-like reactions, Angew. Chem. Int. Ed. 61 (2022), e202207268, https://doi.org/10.1002/anie.202207268.

[22] Z. Jin, P. Li, Y. Meng, Z. Fang, D. Xiao, G. Yu, Understanding the inter-site distance effect in single-atom catalysts for oxygen electroreduction, Nat. Catal. 4 (2021) 615–622, https://doi.org/10.1038/s41929-021-00650-w.

[23] C. Chu, D. Huang, S. Gupta, S. Weon, J. Niu, E. Stavitski, C. Muhich, J.H. Kim, Neighboring Pd single atoms surpass isolated single atoms for selective hydrodehalogenation catalysis, Nat. Commun. 12 (2021) 5179, https://doi.org/10.1038/s41467-021-25526-2.

[24] X. Cheng, H.G. Guo, Y.L. Zhang, X. Wu, Y. Liu, Non-photochemical production of singlet oxygen via activation of persulfate by carbon nanotubes, Water Res. 113 (2017) 80–88, https://doi.org/10.1016/j.watres.2017.02.016.

[25] L. Zhao, Y. Zhang, L.B. Huang, X.Z. Liu, Q.H. Zhang, C. He, Z.Y. Wu, L.J. Zhang, J. P. Wu, W.L. Yang, L. Gu, J.S. Hu, L.J. Wan, Cascade anchoring strategy for general mass production of high-loading single-atomic metal-nitrogen catalysts, Nat. Commun. 10 (2019) 1278, https://doi.org/10.1038/s41467-019-09290-y.

[26] Z.Q. Wang, C.Y. Du, D.H. Ding, R.Z. Chen, S.J. Yang, T.M. Cai, Recent advances in metal-free catalysts for the remediation of antibiotics, antibiotic resistant bacteria (ARB), and antibiotic resistant genes (ARGs), J. Mater. Chem. A 10 (2022) 15235–15266, https://doi.org/10.1039/D2TA03510C.

[27] X.C. Wang, K. Maeda, A. Thomas, K. Takanabe, G. Xin, J.M. Carlsson, K. Domen, M. Antonietti, A metal-free polymeric photocatalyst for hydrogen production from water under visible light, Nat. Mater. 8 (2009) 76–80, https://doi.org/10.1038/nmat2317.

[28] J. Miao, W. Geng, P.J.J. Alvarez, M.C. Long, 2D N-doped porous carbon derived from polydopamine-coated graphitic carbon nitride for efficient nonradical activation of peroxymonosulfate, Environ. Sci. Technol. 54 (2020) 8473–8481, https://doi.org/10.1021/acs.est.0c03207.

[29] B.C. Huang, J. Jiang, G.X. Huang, H.Q. Yu, Sludge biochar-based catalysts for improved pollutant degradation by activating peroxymonosulfate, J. Mater. Chem. A 6 (2018) 8978–8985, https://doi.org/10.1039/C8TA02282H.
[30] X. Wang, X. Liu, H. Wen, K. Guo, H. Brendon, D. Liu, A green, efficient reductive N-formylation of nitro compounds catalyzed by metal-free graphitic carbon nitride supported on activated carbon, Appl. Catal. B: Environ. 321 (2023), 122042, https://doi.org/10.1016/j.apcatb.2022.122042.
[31] R.H. Huang, J.P. Lv, J.B. Chen, Y.L. Zhu, J. Zhu, T. Wagberg, G.Z. Hu, Three-dimensional porous high boron-nitrogen-doped carbon for the ultrasensitive electrochemical detection of trace heavy metals in food samples, J. Hazard. Mater. 442 (2023), 130020, https://doi.org/10.1016/j.jhazmat.2022.130020.
[32] F. Qi, Q. Wang, Z. Zeng, Q. Wen, Z. Huang, Insight into the roles of microenvironment and active site on the mechanism regulation in metal-free persulfate activation process coupling with an electric field, J. Hazard. Mater. 439 (2022), 129673, https://doi.org/10.1016/j.jhazmat.2022.129673.
[33] D.L. Guo, S.J. You, F. Li, Y.B. Liu, Engineering carbon nanocatalysts towards efficient degradation of emerging organic contaminants via persulfate activation: a review, Chin. Chem. Lett. 33 (2022) 1–10, https://doi.org/10.1016/j.cclet.2021.06.027.
[34] Y. Guo, Q.X. Zhou, J. Nan, W.X. Shi, F.Y. Cui, Y.F. Zhu, Perylenetetracarboxylic acid nanosheets with internal electric fields and anisotropic charge migration for photocatalytic hydrogen evolution, Nat. Commun. 13 (2022) 2067, https://doi.org/10.1038/s41467-022-29826-z.
[35] Y. Wu, J. Chen, H.N. Che, X. Gao, Y.H. Ao, P.F. Wang, Boosting 2e$^-$ oxygen reduction reaction in garland carbon nitride with carbon defects for high-efficient photocatalysis-self-Fenton degradation of 2,4-dichlorophenol, Appl. Catal. B: Environ. 307 (2022), 121185, https://doi.org/10.1016/j.apcatb.2022.121185.
[36] K.H. Guo, Z.H. Wu, S.W. Yan, B. Yao, W.H. Song, Z.C. Hua, X.W. Zhang, X.J. Kong, X.C. Li, J.Y. Fang, Comparison of the UV/chlorine and UV/H_2O_2 processes in the degradation of PPCPs in simulated drinking water and wastewater: kinetics, radical mechanism and energy requirements, Water Res. 147 (2018) 184–194, https://doi.org/10.1016/j.watres.2018.08.048.
[37] T. Tsuneda, T. Taketsugu, Theoretical investigations on hydrogen peroxide decomposition in aquo, Phys. Chem. Chem. Phys. 20 (2018) 24992–24999, https://doi.org/10.1039/C8CP04299C.
[38] C. Ling, S. Wu, J. Han, T. Dong, C. Zhu, X. Li, L. Xu, Y. Zhang, M. Zhou, Y. Pan, Sulfide-modified zero-valent iron activated periodate for sulfadiazine removal: performance and dominant routine of reactive species production, Water Res. 220 (2022), 118676, https://doi.org/10.1016/j.watres.2022.118676.
[39] Z.Y. Jin, P.P. Li, Y. Meng, Z.W. Fang, D. Xiao, G.H. Yu, Understanding the inter-site distance effect in single-atom catalysts for oxygen electroreduction, Nat. Catal. 4 (2021) 615–622, https://doi.org/10.1038/s41929-021-00650-w.
[40] C.H. Chu, D.H. Huang, S. Gupta, S. Weon, J.F. Niu, E. Stavitski, C. Muhich, J. H. Kim, Neighboring Pd single atoms surpass isolated single atoms for selective hydrodehalogenation catalysis, Nat. Commun. 12 (2021) 5179, https://doi.org/10.1038/s41467-021-25526-2.
[41] A.F. Wang, P. Zhou, D.Q. Tian, H. Zhang, Z.K. Xiong, Y. Du, C.S. He, Y. Yuan, T. T. Chen, Y. Liu, B. Lai, Enhanced oxidation of fluoroquinolones by visible light-induced peroxydisulfate: The significance of excited triplet state species, Appl. Catal., B Environ. 316 (2022), 121631, https://doi.org/10.1016/j.apcatb.2022.121631.
[42] L.W. Gao, Y. Guo, J.H. Zhan, G. Yu, Y.J. Wang, Assessment of the validity of the quenching method for evaluating the role of reactive species in pollutant abatement during the persulfate-based process, Water Res. 221 (2022), 118730, https://doi.org/10.1016/j.watres.2022.118730.
[43] X.J. Xu, D.D. Tang, J.H. Cai, B.D. Xi, Y. Zhang, L. Pi, X.H. Mao, Heterogeneous activation of peroxymonocarbonate by chalcopyrite ($CuFeS_2$) for efficient degradation of 2,4-dichlorophenol in simulated groundwater, Appl. Catal. B: Environ. 251 (2019) 273–282, https://doi.org/10.1016/j.apcatb.2019.03.080.
[44] M. Yang, K.Y. Wu, S.D. Sun, J.L. Duan, X. Liu, J. Cui, S.H. Liang, Y.J. Ren, Unprecedented relay catalysis of curved Fe_1-N_4 single-atom site for remarkably efficient $^1O_2$ generation, ACS Catal. 13 (2022) 681–691, https://doi.org/10.1021/acscatal.2c05409.
[45] Y.N. Zhang, D. Wang, W.X. Liu, Y. Lou, Y. Zhang, Y.M. Dong, J. Xu, C.S. Pan, Y. F. Zhu, Create a strong internal electric-field on PDI photocatalysts for boosting phenols degradation via preferentially exposing pi-conjugated planes up to 100 %, Appl. Catal. B: Environ. 300 (2022), 120762 https://doi.org/10.1016/j.apcatb.2021.120762.
[46] G.V. Buxton, C.L. Greenstock, W.P. Helman, A.B. Ross, Critical-review of rate constants for reactions of hydrated electrons, hydrogen-atoms and hydroxyl radicals ($^{\cdot}OH/^{\cdot}O^-$) in aqueous-solution, J. Phys. Chem. Ref. Data 17 (1988) 513–886, https://doi.org/10.1063/1.555805.
[47] X. Cheng, H.G. Guo, W. Li, B. Yang, J.Q. Wang, Y.L. Zhang, E.D. Du, Metal-free carbocatalysis for persulfate activation toward nonradical oxidation: Enhanced singlet oxygen generation based on active sites and electronic property, Chem. Eng. J. 396 (2020), 125107, https://doi.org/10.1016/j.cej.2020.125107.
[48] S.Y. Wang, H.J. Jiao, Scavenging capacity of berry crops on superoxide radicals, hydrogen peroxide, hydroxyl radicals, and singlet oxygen, J. Agr. Food Chem. 48 (2000) 5677–5684, https://doi.org/10.1021/jf000766i.
[49] Y.W. Gao, Z.H. Chen, Y. Zhu, T. Li, C. Hu, New insights into the generation of singlet oxygen in the metal-free peroxymonosulfate activation process: Important role of electron-deficient carbon atoms, Environ. Sci. Technol. 54 (2020) 1232–1241, https://doi.org/10.1021/acs.est.9b05856.
[50] Y.Q. Wang, K. Li, M.Y. Shang, Y.Z. Zhang, Y. Zhang, B.L. Li, Y.J. Kan, X.Q. Cao, J. Zhang, A novel partially carbonized Fe_3O_4@PANI-p catalyst for tetracycline degradation via peroxymonosulfate activation, Chem. Eng. J. 451 (2023), 138655, https://doi.org/10.1016/j.cej.2022.138655.
[51] C.C. Dong, Z.Q. Wang, Z.C. Ye, J.H. He, Z.X. Zheng, X.Q. Gong, J.L. Zhang, I.M. C. Lo, Superoxide radicals dominated visible light driven peroxymonosulfate activation using molybdenum selenide ($MoSe_2$) for boosting catalytic degradation of pharmaceuticals and personal care products, Appl. Catal. B: Environ. 296 (2021), 120223, https://doi.org/10.1016/j.apcatb.2021.120223.
[52] L.H. Wang, H.D. Xu, N. Jiang, Z.M. Wang, J. Jiang, T. Zhang, Trace cupric species triggered decomposition of peroxymonosulfate and degradation of organic pollutants: Cu(III) being the primary and selective intermediate oxidant, Environ. Sci. Technol. 54 (2020) 4686–4694, https://doi.org/10.1021/acs.est.0c00284.
[53] P.G. Tratnyek, J. Holgne, Oxidation of substituted phenols in the environment - a qsar analysis of rate constants for reaction with singlet oxygen, Environ. Sci. Technol. 25 (1991) 1596–1604, https://doi.org/10.1021/es00021a011.
[54] Y. Bao, C. Lian, K. Huang, H.R. Yu, W.Y. Liu, J.L. Zhang, M.Y. Xing, Generating high-valent iron-oxo equivalent to $=Fe^{IV}=O$ complexes in neutral microenvironments through peroxymonosulfate activation by Zn-Fe layered double hydroxides, Angew. Chem. Int. Ed. 61 (2022), e202209542, https://doi.org/10.1002/anie.202209542.
[55] J.J. Li, S.M. Ma, Z.Y. Qi, J. Ding, M.H. Yin, B. Zhao, Z.H. Zhang, Y. Wang, H. W. Zhang, L. Wang, D.D. Dionysiou, Insights into the removal of chloramphenicol by electrochemical reduction on Pd/NiFe-MOF/foam-Ni electrode: Performance and mechanism, Appl. Catal. B: Environ. 322 (2023), 122076, https://doi.org/10.1016/j.apcatb.2022.122076.
[56] Y.Y. Chu, X.L. Zheng, J.R. Fan, Preparation of sodium and boron co-doped graphitic carbon nitride for the enhanced production of H_2O_2 via two-electron oxygen reduction and the degradation of 2,4-DCP via photocatalytic oxidation coupled with Fenton oxidation, Chem. Eng. J. 431 (2022), 134020, https://doi.org/10.1016/j.cej.2021.134020.